Tropical Plants

ARTICLE

Open Access

https://doi.org/10.48130/tp-0025-0028

Tropical Plants **2025**, 4: e034

Predominance of the ASP-104 site of fatty acid desaturase 3 promoted a linolenic acid (ALA) accumulation in *Plukenetia volubilis*

Authors

Yijun Fu[#], Zhaohui Wang[#], Lixuan Ye, Guofang Deng, Kexian Li, ..., Jun Niu[*]

Correspondence

niujun@hainanu.edu.cn

In Brief

Plukenetia volubilis fatty acid desaturase 3 (*PvFAD3*) is essential for α-linolenic acid (ALA) biosynthesis. Bioinformatics analysis indicated that the aspartate at position 104 (ASP-104) of *PvFAD3* was a potential key site. Through *in vitro* site-directed mutagenesis, the ASP-104 was converted to asparagine, generating the mutant *PvFAD3* (m*PvFAD3*). Using two methods, transgenic yeast and transgenic *Arabidopsis*, it was proved that the ASP-104 site could affect ALA accumulation. Our work provides mechanistic insights into FAD3 function and enables targeted genetic strategies for enhancing ALA production in oil plants.

Graphical abstract

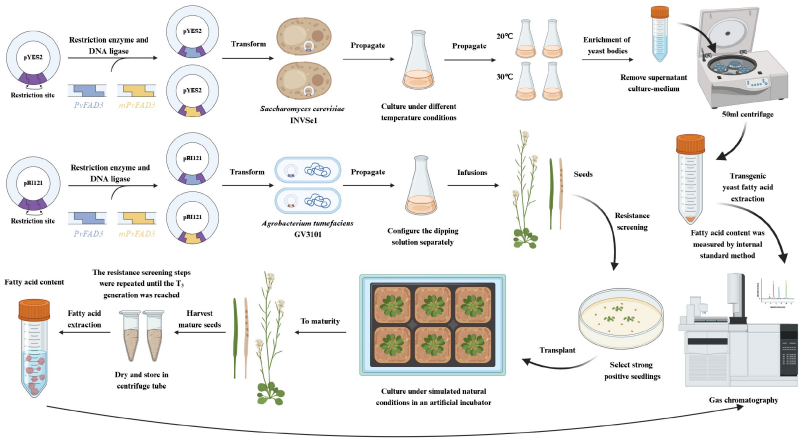

Highlights

- The key active site residue of the PvFAD3 protein was identified as ASP-104 by molecular docking methods.
- Significant reduction of ALA content was found in transgenic m*PvFAD3* yeast compared to *PvFAD3*.
- Significant reduction of ALA content was found in transgenic m*PvFAD3 Arabidopsis thaliana* seeds compared to *PvFAD3*.

Citation: Fu Y, Wang Z, Ye L, Deng G, Li K, et al. 2025. Predominance of the ASP-104 site of fatty acid desaturase 3 promoted a linolenic acid (ALA) accumulation in *Plukenetia volubilis*. *Tropical Plants* 4: e034 https://doi.org/10.48130/tp-0025-0028

Tropical Plants

ARTICLE

Open Access

https://doi.org/10.48130/tp-0025-0028

Tropical Plants **2025**, 4: e034

Predominance of the ASP-104 site of fatty acid desaturase 3 promoted a linolenic acid (ALA) accumulation in *Plukenetia volubilis*

Yijun Fu[#], Zhaohui Wang[#], Lixuan Ye, Guofang Deng, Kexian Li, Yuan Zou, Jia Wang and Jun Niu[*]

Key Laboratory of Genetics and Germplasm Innovation of Tropical Special Forest Trees and Ornamental Plants - Ministry of Education, School of Tropical Agriculture and Forestry, Hainan University, Haikou, Hainan 570228, China

[#] Authors contributed equally: Yijun Fu, Zhaohui Wang

[*] Corresponding author, E-mail: niujun@hainanu.edu.cn

Abstract

Plukenetia volubilis is a perennial oilseed plant with high α-linolenic acid (ALA) content. Although fatty acid desaturase 3 (FAD3) is essential for ALA biosynthesis, its structural determinants and functional mechanisms remain unclear. This study employed molecular docking and bioinformatics to identify the aspartate at position 104 (ASP-104), as a pivotal residue in *P. volubilis* FAD3 (PvFAD3). Through *in vitro* site-directed mutagenesis, ASP-104 was converted to asparagine, generating the mutant *PvFAD3* (m*PvFAD3*). Compared to yeast expressing *PvFAD3,* the m*PvFAD3* expression showed 32.60% and 77.27% reductions in ALA content at 30 °C and 20 °C, respectively. Complementation assays revealed that heterologous expression of m*PvFAD3* resulted in a 65.52% decrease in seed ALA content when compared to *Arabidopsis thaliana* seeds transformed with *PvFAD3*. These results conclusively demonstrate that ASP-104 is a critical site positively regulating PvFAD3 activity, with the mutation leading to a significant decline in ALA synthesis. The present work provides mechanistic insights into FAD3 function, enabling targeted genetic strategies for enhancing ALA production in oil crops.

Citation: Fu Y, Wang Z, Ye L, Deng G, Li K, et al. 2025. Predominance of the ASP-104 site of fatty acid desaturase 3 promoted a linolenic acid (ALA) accumulation in *Plukenetia volubilis*. *Tropical Plants* 4: e034 https://doi.org/10.48130/tp-0025-0028

Introduction

Plukenetia volubilis, belonging to the Euphorbiaceae family, is a perennial woody liana renowned for its significant economic value. Cultivated as an oilseed crop in South America[1,2], it yields approximately 1,200 tons of seeds annually in Peru[3]. In China, *P. volubilis* is recognized as an emerging economic crop, cultivated extensively in subtropical and tropical regions such as Guangdong, Yunnan, and Hainan provinces[4]. Mature *P. volubilis* seeds (PVS) contain approximately 50% oil by weight[5]. The predominant fatty acids (FAs) are palmitic acid (C16:0), stearic acid (C18:0), oleic acid (C18:1), linoleic acid (C18:2, LA), and linolenic acid (C18:3, ALA)[6]. Notably, the essential FAs of LA and ALA constitute approximately 25% and 50% of total FAs, respectively[7]. As essential nutrients, LA and ALA cannot be endogenously synthesized in humans due to the lack of Δ15-desaturase and must be acquired through dietary sources[8]. As the downstream metabolites of ALA, eicosapentaenoic acid and docosahexaenoic acid exhibit a wide array of biological activities beneficial for human health[9]. These compounds show preventive effects against various disorders, including coronary heart disease[10], hypertension, diabetes, arthritis, high cholesterol, cancer, and autoimmune diseases. Consequently, the ALA content serves as a key quality indicator for edible oils. Developing high-ALA varieties represents a major objective in oil crop breeding.

Fatty acid desaturase 3 (FAD3) is a key enzyme in ALA biosynthesis and functions as the rate-limiting step[11]. FAD3 activity is regulated by its catalytic center structure, enzyme-substrate affinity, and protein conformational stability[12]. FAD3 proteins exhibit conserved structural features and high sequence homology among diverse species. Initially cloned from *Arabidopsis thaliana*, the *FAD3* gene has been subsequently identified in various plants, including *P. volubilis*, *Perilla frutescens*, *Glycine max*, and *Carthamus tinctorius*[13–16]. Heterologous overexpression of the *Jatropha curcas FAD3* (*JcFAD3*) gene significantly increases ALA accumulation in *A. thaliana* seeds[17]. The *FAD3* expression markedly increases ALA content in the yeast mutant (H1246)[18]. Notably, elevated *FAD3* expression in seeds strongly correlates with ALA accumulation, including in *P. volubilis*[19]. Transcriptome analysis reveals a direct relationship between ALA content and *P. volubilis FAD3* (*PvFAD3*) expression[20]. Furthermore, heterologous *PvFAD3* overexpression enhances ALA synthesis in *Nicotiana benthamiana* seeds[19]. Overall, *FAD3* expression directly influences ALA accumulation in plant seeds, underscoring its crucial role in the regulation of ALA synthesis. However, current PvFAD3 research has mainly examined its expression effects on ALA levels and regulatory networks, whereas structural studies on its catalytic mechanism remain limited.

Certain conserved amino acid positions, at or near the catalytic center, can exert profound influences on enzyme stability, function, and activity[12]. For example, the E6V mutation in hemoglobin's β-subunit causes sickle cell anemia[21]. Site-directed mutagenesis of TesA thioesterase significantly enhanced octanoic acid (C8:0) production via the Type II fatty acid synthesis pathway[22]. Contemporary methods, including functional domain exchange, site-specific mutation, and bioinformatics, are employed to explore the intricate relationship between enzyme structure and function[23,24]. In plants, membrane-bound FAD3 exhibits greater structural complexity than soluble proteins[25]. Thus, this complexity impedes FAD3 purification, limiting applications of cryo-electron microscopy and nuclear magnetic resonance techniques. Currently, limited research on the crystal structure of Δ9 fatty acid desaturase (belonging to the same family as FAD3) in humans and mammals has indicated the presence of four hydrophobic transmembrane structures[26,27]. This finding serves as a valuable reference for studying the structure and function of FAD3. Plant FAD3 contains 3–4 transmembrane domains (TM1–TM4) and two amphipathic helices (AH1–AH2)[25]. Importantly, three conserved histidine clusters (HX_3H in the His-boxI region, HX_2HH in the His-boxII, and His-boxIII regions) coordinate non-heme Fe^{2+}, essential for FAD3 activity[25]. Despite

these insights, limited reports explore the relationship between the structure of the FAD3 enzyme and its catalytic function. Additional studies are needed to elucidate this mechanism.

In this investigation, a comprehensive approach involving homology modelling, model evaluation, conserved domain prediction, and homology sequence comparison analysis was employed to predict the pivotal sites influencing the activity of the PvFAD3 protein. Using site-directed mutagenesis via the bypass method, a mutant *PvFAD3* (m*PvFAD3*) variant was generated, and key residues in PvFAD3 were substituted. To assess the impact of this substitution on enzyme activity, both *PvFAD3* and m*PvFAD3* were overexpressed in *Saccharomyces cerevisiae*, and replacement experiments were conducted in *A. thaliana FAD3* mutants (*AtFAD3*m). Gas chromatography-mass spectrometry (GC-MS) revealed the influence of key sites on PvFAD3 activity. Identifying these critical PvFAD3 residues advances our understanding of fatty acid desaturase mechanisms and enables novel oil crop improvement strategies.

Materials and methods

Plant material

Mature PVS samples were sourced from the plantation base of Hainan University, located in Danzhou, Hainan, China (Fig. 1; longitude and latitude: 109.503179, 19.542727)[20]. Post-collection, fruits were meticulously peeled, and the seeds were extracted, promptly frozen in liquid nitrogen, and stored at −80 °C for future use.

The T-DNA insertion line *FAD3* silencing mutant *A. thaliana* (SALK_071996C) was procured from AraShare (www.arashare.cn). Subsequent to germination, the seeds were cultivated in a controlled environment within an artificial climate incubator, main-taining conditions of 23 °C, 60% humidity, light intensity ranging from 100−150 μmol/m^2/s, and a light period of 16 h, followed by 8 h of darkness.

Homology modelling and molecular docking

The *PvFAD3* gene sequence was extracted from previous transcriptome data of *P. volubilis*[20]. The amino acid sequence of PvFAD3 was obtained using SnapGene software. The tertiary structure of PvFAD3 was predicted using the Phyre2 online prediction tool (www.sbg.bio.ic.ac.uk/phyre2). To validate the reliability of the predicted model, the SAVES online server (https://saves.mbi.ucla.edu/) was employed. The three-dimensional data structure of the substrate LA was retrieved from the PubChem database (https://pubchem.ncbi.nlm.nih.gov/). AutoDock Tools (ADT) was utilized for processing, resulting in the generation of a ligand structure file. The PvFAD3 simulated protein was dehydrated and hydrogenated using ADT software to maintain the original charge, designating it as the receptor structure. Further, ADT was employed to conduct rigid docking of small ligand molecules to the receptor. The grid box size were set to 30 Å × 30 Å × 30 Å, with a typical grid spacing of 0.375 Å. Ultimately, the tertiary structure of PvFAD3 was analyzed using SPDBV software.

Homologous sequence comparison

To assess the homology of FAD3 proteins, a search was conducted using the NCBI database (www.ncbi.nlm.nih.gov/). A total of 26 protein sequences homologous to PvFAD3 were selected (Supplementary Table S1). The conserved domain within the full-length amino acid sequence of FAD3 was predicted using the MEME online tool (http://meme-suite.org/). The full-length amino acid sequences of 27 FAD3, including PvFAD3, were compared and analyzed using DNAMAN software.

Topological structure analysis of PvFAD3

Protein hydrophilicity and hydrophobicity of PvFAD3 was analyzed using DNAMAN software. The TMHMM online program (www.cbs.dtu.dk/services/TMHMM/) was utilized to predict the PvFAD3 topology information across the membrane structure. Based on the aforementioned information, the topological model for PvFAD3 proteases was constructed.

Objective gene acquisition and construction of an expression vector

Based on the gene sequences of *PvFAD3*, specific primers (Supplementary Table S2) were designed to obtain the full-length gene of *PvFAD3*. The gene sequence of m*PvFAD3* was obtained using a 'bypass method' (Supplementary Fig. S1). By introducing the gene sequences of *PvFAD3* and m*PvFAD3* into the pYES2 vector treated with *Eco*RI and *Hind*III endonucleases, the recombinant vectors pYES2-*PvFAD3* and pYES2-m*PvFAD3* were generated (Supplementary Fig. S2). Similarly, by incorporating the gene sequences of *PvFAD3* and m*PvFAD3* into the pBI121 vector treated with *Xba*I and *Sac*I endonucleases, the recombinant vectors pBI121-*PvFAD3* and pBI121-m*PvFAD3* were obtained. The resulting recombinant vector was sent to Hainan Nanshan Biotechnology Company (Hainan, China) for sequencing, and stored at −20 °C for future use.

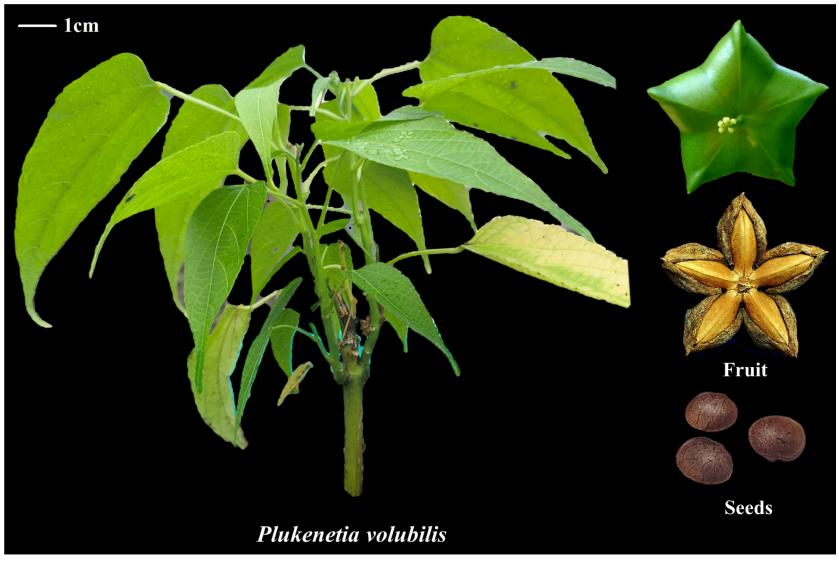

Fig. 1 Phenotypes of *Plukenetia volubilis* and its fruits.

Transgenic yeast culture

Yeast transformation was conducted employing thermal stimulation, with transgenic *S. cerevisiae* strains harboring the empty pYES2 vector as the negative control. Transgenic *S. cerevisiae* strains carrying the recombinant vectors pYES2-*PvFAD3* and pYES2-m*PvFAD3* underwent inoculation in SD-Ura liquid medium for activation culture. Under aseptic conditions, bacteria were collected through centrifugation and then inoculated into SG/-Ura liquid medium containing 1% raffinose at a ratio of 1:100. Subsequently, 50 μL of LA with a final concentration of 300 μg/mL was added, and 1% surfactant IGE-PAL CA-630 was included in the medium to emulsify LA and facilitate its cellular entry. The yeast was cultured at 28 °C and 180 rpm in a shaker, and at 5 °C and 180 rpm in a separate shaker for 36 to 72 h until reaching a stable stage. Yeast cells were then collected by centrifugation at 5,000 rpm, washed three times with deionized water, dried using a vacuum freeze dryer, and stored at −80 °C for future use. Three parallel samples were prepared for the experiment.

Arabidopsis mutant replacement

The *AtFAD3*m seeds were sown and nurtured for robust growth. The three-primer method was used to identify mutant homozygotes (Supplementary Table S2). Homozygous *AtFAD3*m seeds were subsequently cultivated, and the *PvFAD3* and m*PvFAD3* genes were integrated into the *Arabidopsis* genome using *Agrobacterium*-mediated transformation. Transgenic positive seedlings were chosen on a 1/2MS plate supplemented with 50 μg/mL Kanamycin ($Kana^+$), and DNA extracted from these seedlings underwent PCR verification using specified primers (Supplementary Table S2). After screening until the T_3 generation, 20 mg of seeds were collected and weighed for subsequent FA extraction and detection.

RT-qPCR validation

Total RNA was isolated using the RNeasy Plant Mini Kit (Qiagen, Germany), followed by cDNA synthesis with the GoScript Reverse Transcription System (Promega, USA). AtACT2 (AT3G18780) served as the endogenous control, as previously established[28]. RT-qPCR was performed using ChamQ Universal SYBR qPCR Master Mix (Vazyme, China), on a LightCycler 96 system (Roche, Switzerland). Primer sequences are provided in Supplementary Table S3. Three technical replicates were analyzed, with relative expression levels calculated using the $2^{-\Delta\Delta CT}$ method.

FA extraction and detection

Heptadecanoic methyl ester (ANPEL, Shanghai, China), and GLC Mixture (ZZSRM, Shanghai, China) were used as the internal and external standards, respectively. An Agilent 6,890 gas chromatograph with a flame ion chromatograph detector was used for analysis. Column box operation procedure: 50 °C for 1 min, 10 °C/min rising to 150 °C for 1 min, and then 4 °C/min rising to 250 °C for 3 min. The sample was loaded with an automatic injector with a loading volume of 1 μL and a split ratio of 50:1. Helium was used as a carrier gas with a flow rate of 1 mL/min.

Using GC-MS data analysis software, fatty acid methyl ester (FAME) standard samples (ANPEL, Shanghai, China) were employed as references to compare the retention times and peak areas of a mixed FAME solution and heptadecane methyl. The percentage composition of fatty acid components was then calculated using the area normalization method. The FA methyl ester samples of transgenic yeast and *A. thaliana* seeds were analyzed qualitatively and quantitatively. Statistical software GraphPad Prism version 8.0.2.263 was used to analyze the significance of differences. The statistical method employed was one-way ANOVA, and a p-value < 0.05 indicated statistically significant differences among the groups.

Results

Homologous modelling and molecular docking

The tertiary structure of PvFAD3 was generated using the Phyre2 online server. The prediction showed 99.8% confidence for template c4zyoA as the PvFAD3 structural model (Fig. 2a). Model quality was assessed through the SAVES online server. The pull diagram results indicated that 97% of the amino acid residues in the c4zyoA model conformed to stereochemical rules within the allowed region (Fig. 2b), confirming its suitability for subsequent analyses. The three-dimensional structure of the substrate LA was obtained from the PubChem database (Fig. 2c). Molecular docking was performed using ADT software after structure preparation. Rigid docking of LA with the PvFAD3 model simulated their binding interaction (Fig. 2d). Docking results suggested mutual induction, deformation, and adaptation between the LA ligand and PvFAD3 mimic protein (Fig. 2d–f). Interestingly, the LA ligand formed a hydrogen bond with the aspartate at position 104 (ASP-104) of the PvFAD3 mimic protein (Fig. 2e, f). Furthermore, hydrogen bond analysis between amino acid residues indicated a bond between ASP-104 and asparagine at position 109 (ASN-109) of the PvFAD3 mimic protein (Fig. 2g). These findings imply that ASP-104 may play a crucial role in protein stability, substrate binding, and potentially have a significant impact on enzyme function.

Prediction analysis of conserved domains

To further evaluate the impact of ASP-104 on FAD3 function, 27 FAD3 homologs were analyzed across diverse species. Three conserved motifs were identified: motif 1 (positioned between 18–67), motif 2 (positioned between 96–145), and motif 3 (positioned between 262–310) (Supplementary Fig. S3). Notably, Asp104 and Asn109 localize within conserved motif 2, comprising the critical region for PvFAD3 protease activity (Fig. 3a). Multiple sequence alignment highlighted the conservation of ASN-109 across all species, while ASP-104 exhibited relative conservation (Fig. 3b). Intriguingly, these species with higher ALA content (such as *P. volubilis*, *Perilla frutescens*, *Paeonia suffruticosa*, etc.) possess aspartate at position 104, whereas these species with lower ALA content (such as *Arachis hypogaea*, *Juglans regia*, *Prunus armeniaca*, etc.) have asparagine or glutamate at position 104 (Fig. 3b). This correlation establishes Asp-104 as a determinant of FAD3 catalytic efficiency.

Topological structure analysis of PvFAD3

To construct a topological model of PvFAD3 protein, the analysis of hydrophilic regions, hydrophobic regions, and transmembrane structure was performed. Combined hydrophilicity/hydrophobicity (Supplementary Fig. S4), and transmembrane domain (Fig. 4a) predictions yielded the PvFAD3 topological model (Fig. 4b). The PvFAD3 protein displayed three non-signal peptide transmembrane structures (TM1, TM2, and TM3), along with two inlay membrane structures (AH1 and AH2), and three conserved histidine regions (1 HX_3H and 2 HX_2HH, known as His-boxI, II, and III) (Fig. 4b). The catalytic His-box motifs localize to the cytoplasmic side of the endoplasmic reticulum membrane (Fig. 4b). The ASP-104 site of the PvFAD3 protein was identified within the AH1 membrane structure, situated between the active regions of His-boxI and His-boxII.

In vitro verification of ASP-104 for PvFAD3 activity

To investigate the impact of ASP-104 on PvFAD3 activity, aspartate was substituted with asparagine at position 104. *PvFAD3* and m*PvFAD3* were both cloned into a pYES2 vector and transformed into *S. cerevisiae* (Supplementary Figs S5–S10). In the control group, the main FA components were monounsaturated FAs (Table 1). Compared with *PvFAD3* transgenic yeasts, m*PvFAD3*-transformed

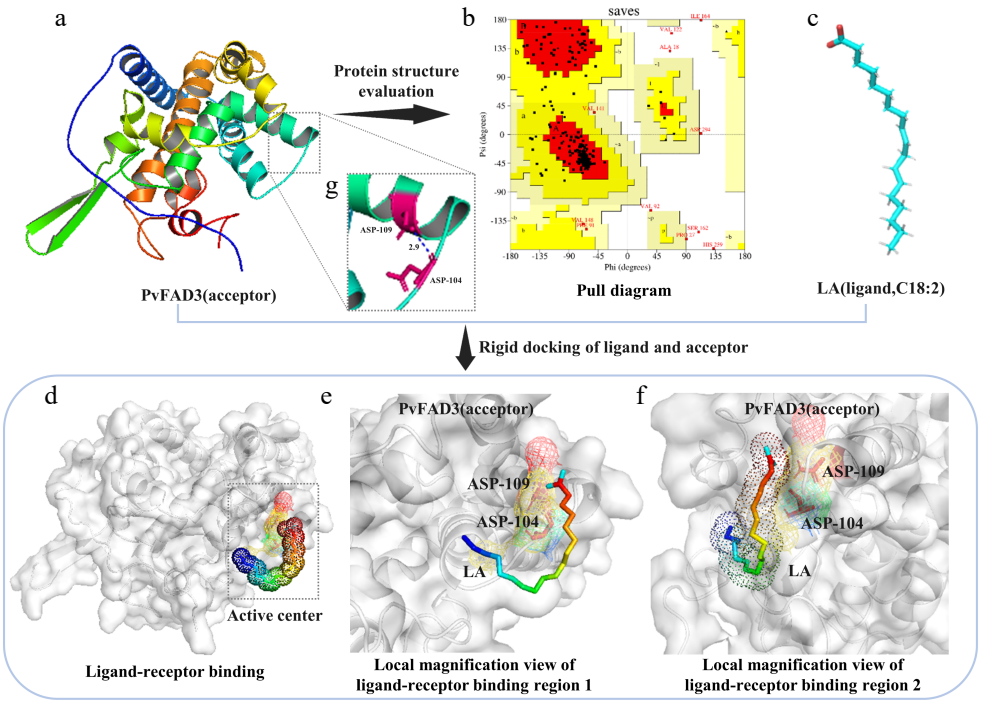

Fig. 2 Model prediction and molecular docking. (a) PvFAD3 tertiary structure prediction. (b) The reliability of the predicted model was evaluated. The Ramachandran plot results showed that 84.1% of the amino acids in the PvFAD3 protein model were located in the most favored region (red region), 11.6% in other allowed regions (yellow region), 1.3% in generally allowed regions (light brown region), and 3% in disallowed regions (white region). If the proportion of amino acid residues falling within the allowed region of the protein model is higher than 90%, the conformation of the model can be considered to conform to the principles of stereochemistry. (c) The tertiary structure of ligand LA. (d) Substrate protein docking prediction. The dashed rectangular region represents the rigid docking active site. (e) Top view of ligand LA small molecule binding to PvFAD3 mimicking protein. (f) Side-view magnification of ligand LA small molecule binding to PvFAD3 mimicking protein. The LA ligand molecule forms hydrogen bonds with the side chain R group of ASP-104 in the simulated PvFAD3 protein. (g) The intramolecular structure of the PvFAD3 protein model was analyzed. The amino acid residues at positions 104 (ASP-104) and 109 (ASN-109) were connected by hydrogen bonds.

yeasts had a similar FA profile with the control group (Table 1). For example, there was a slight difference in C14:0, C16:0, C16:1, C18:0, and C18:1 contents between m*PvFAD*3-transformed yeasts and the control group (Table 1). Interestingly, the expression of *PvFAD3* resulted in a significant several-fold accumulation of saturated FAs, such as C14:0 and C16:0 (Table 1).

The primary focus lies in the alterations in ALA content. Under cultivation at 30 °C, the ALA (C18:3) content in *PvFAD3*- and m*PvFAD3*-transformed yeasts increased by 8.49% and 6.56%, respectively, compared with the control group (Table 1). Under 20 °C cultivation conditions, *PvFAD3*- and m*PvFAD3*-transformed yeasts exhibited increases of 15.52% and 5.06%, respectively (Table 1). Although both *PvFAD3* and m*PvFAD3* expressions increased ALA production, wild-type PvFAD3 showed significantly greater enhancement (Table 1). Notably, when cultivated at 20 °C, the ALA content in *PvFAD3*-transformed yeasts was three times higher than that in m*PvFAD3*-transformed yeasts (Table 1). These findings illustrate the ability for PvFAD3 to effectively enhance ALA accumulation at 20 °C.

In vivo verification of ASP-104 for PvFAD3 activity

Homozygous *Atfad3* mutants were genotyped using a three-primer PCR strategy (Fig. 5a). *PvFAD3* and m*PvFAD3* were cloned into the pBI121 vector and transformed into homozygous *AtFAD3*m. Through resistance selection and PCR analysis, complementation lines for *PvFAD3* and m*PvFAD3* were screened (Fig. 5b–e). The RT-qPCR demonstrated that there is no significant difference in the expression levels of *PvFAD3* and m*PvFAD3* in their respective corresponding *A. thaliana* strains (Fig. 5f). It was obvious that *PvFAD3* and m*PvFAD3* complementation lines exhibit more robust growth phenotypes compared to *AtFAD3*m (Fig. 5f, g). Compared with *AtFAD3*m seeds (16.18%), total oil contents were significantly increased in *PvFAD3* (22.60%) and m*PvFAD3* (20.53%) complementation lines (Table 2). The FA composition analysis showed that *PvFAD3* complementation seeds had a significant increase in the average content of C18:2, C18:3, C20:0, and C20:1, with improvements of 39.80%, 63.27%, 38.89%, and 42.90%, respectively (Table 2). The m*PvFAD3* complementation seeds exhibited a significant increase in the average content of C18:2 and C20:0, with improvements of 25.71% and 20.24%, respectively (Table 2). Importantly, when compared with *AtFAD3*m lines, the *PvFAD3* complementation lines demonstrated a significant increase in C18:3 content, while m*PvFAD3* complementation lines displayed no significant change (Table 2).

Discussion

As an essential ω-3 fatty acid obtained from plant oils, ALA plays vital physiological roles in humans. ALA not only contributes to lowering hypertension and hypertriglyceridemia, but also undergoes conversion into eicosapentaenoic acid and 3-series prostaglandins within the body[29,30]. The consumption of vegetable oils rich in ALA has been linked to significant cardiovascular benefits[29]. ALA-enriched oils are increasingly incorporated into human diets globally. Recognized as a perennial woody oil plant, *P. volubilis* yields a high content of polyunsaturated FAs, particularly rich in ALA[31]. Although the ALA content of PVS oil is slightly lower than that of linseed oil, it significantly surpasses that of commonly used edible oils, including peanut oil, maize oil, rapeseed oil, and olive

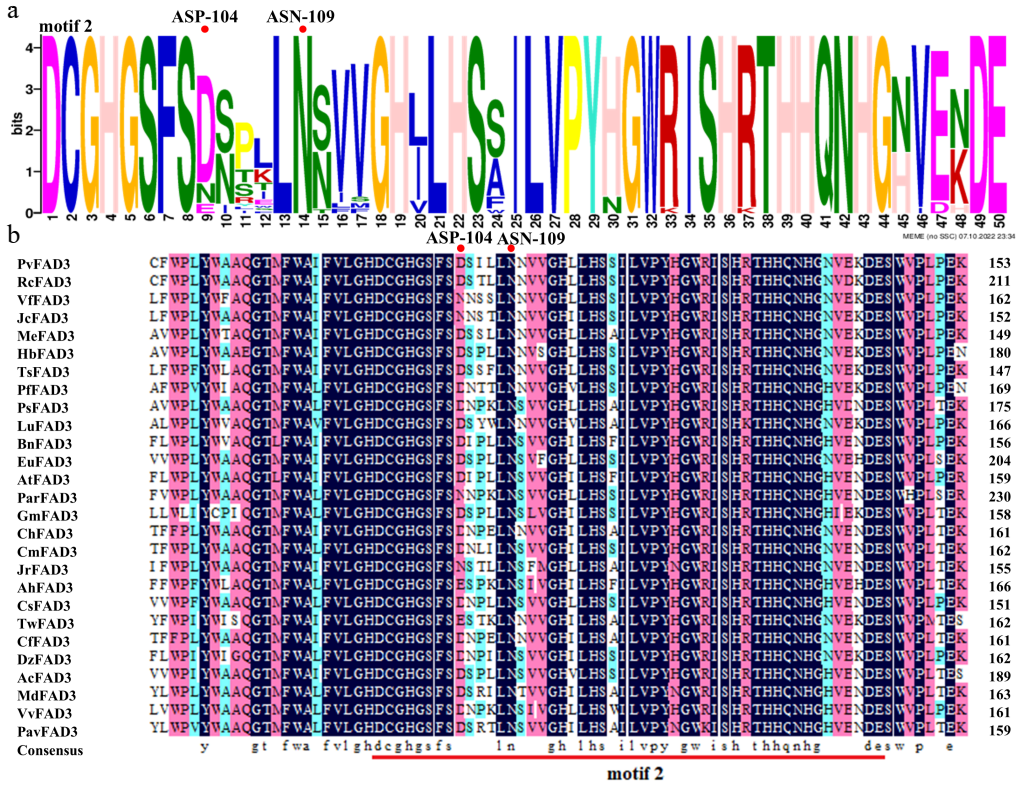

Fig. 3 Conserved domains are predicted by homologous sequence alignment. (a) ASP-104 and ASN-109 are located in the PvFAD3 protein conserved domain motif 2. The larger the letter font, the more conserved the site. (b) The comparison of FAD3 proteins in 27 different species. There were significant differences in ASP-104 among different species, while ASN-109 was absolutely conserved. Dark blue: amino acid homology = 100%, Pink: amino acid homology ≥ 75%, Light blue: amino acid homology ≥ 50%. RcFAD3, EEF36775.1; VfFAD3, AAC98967.2; JcFAD3, NP_001292929.1; MeFAD3, XP_021610352.1; MeFAD3, XP_021610352.1; HbFAD3, XP_021666224.1; TsFAD3, ABM68629.1; PfFAD3, AQZ42316.1; PsFAD3, AVZ47050.1; LuFAD3, BAG70950.1; BnFAD3, AAT09135.1; EuFAD3, ARQ20744.1; AtFAD3, NP_180559.1; ParFAD3, CAB4284757.1; GmFAD3, NP_001236114.1; ChFAD3, AEF80000.1; CmFAD3, KAF3952997.1; JrFAD3, XP_018835457.1; AhFAD3, QBI71562.1; CsFAD3, XP_028086292.1; TwFAD3, XP_038705526.1; CfFAD3, KAE8039281.1; DzFAD3, XP_022756628.1; AcFAD3, PSS09495.1; MdFAD3, XP_008384790.2; VvFAD3, XP_002277573.1; PavFAD3, XP_021816263.1.

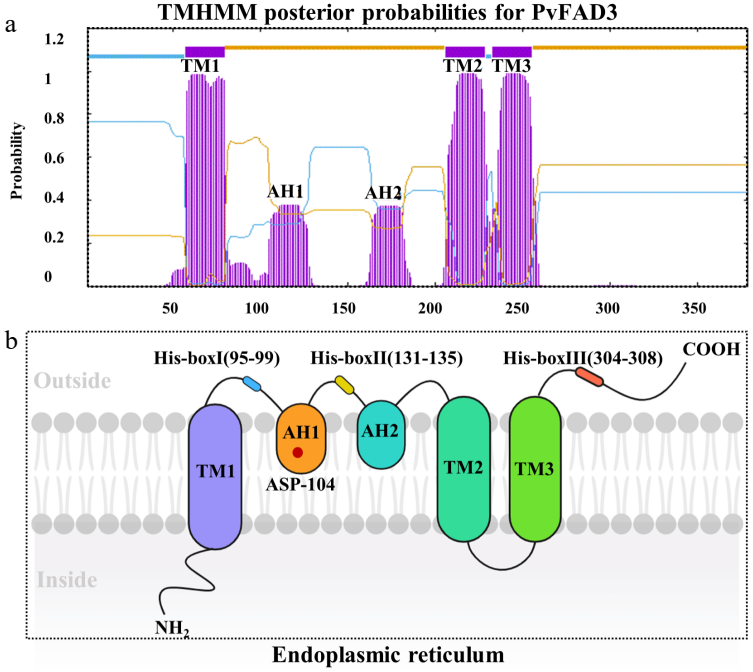

Fig. 4 The topological model of PvFAD3. (a) PvFAD3 protein cross membrane structure prediction. The purple structure represents a cross-membrane or inlaid protein structure. (b) Topological model prediction of PvFAD3 proteins. TM1, TM2, and TM3: Protein transmembrane structure. AH1 and AH2: Protein mosaic structure. His-boxI, His-boxII, and His-boxIII: Histidine active region. Red Star: ASP-104.

Table 1. Fatty acid compositions in different yeasts.

Culture condition	Group	FA components (%)						
		C14:0	C16:0	C16:1	C18:0	C18:1	C18:2	C18:3
30 °C	pYES2	1.28 ± 0.34^{c}	12.16 ± 0.76^{e}	43.12 ± 0.61^{a}	2.82 ± 0.06^{c}	21.36 ± 0.65^{a}	19.26 ± 0.40^{c}	0.00 ± 0.00^{e}
	pYES2-*PvFAD3*	12.63 ± 0.45^{a}	44.03 ± 0.54^{b}	6.24 ± 0.08^{c}	1.59 ± 0.04^{d}	9.87 ± 0.55^{c}	17.14 ± 0.64^{d}	8.49 ± 0.09^{b}
	pYES2-m*PvFAD3*	1.67 ± 0.07^{c}	15.27 ± 0.53^{d}	42.23 ± 0.49^{a}	4.15 ± 0.06^{b}	22.77 ± 0.55^{a}	7.35 ± 0.39^{e}	6.56 ± 0.17^{c}
20 °C	pYES2	0.00 ± 0.00^{d}	15.98 ± 0.30^{d}	29.01 ± 0.42^{b}	4.53 ± 0.22^{a}	14.09 ± 0.76^{b}	36.39 ± 0.71^{a}	0.00 ± 0.00^{e}
	pYES2-*PvFAD3*	10.99 ± 0.23^{b}	62.04 ± 0.34^{a}	1.42 ± 0.15^{d}	1.33 ± 0.07^{d}	6.78 ± 0.43^{d}	1.92 ± 0.28^{f}	15.52 ± 0.32^{a}
	pYES2-m*PvFAD3*	1.94 ± 0.22^{c}	18.50 ± 0.54^{c}	28.09 ± 0.43^{b}	4.66 ± 0.05^{a}	19.64 ± 0.68^{a}	22.10 ± 0.44^{b}	5.06 ± 0.47^{d}

Different letters indicate significant differences ($p < 0.05$).

oil[7]. Remarkably, *P. volubilis*, being a perennial plant, allows for multiple harvests with a single planting and does not require arable land. Consequently, *P. volubilis* has emerged as a novel and economically valuable oil crop in southern China. Research has consistently demonstrated that FAD3 serves as the principal rate-limiting enzyme in ALA biosynthesis[11]. Previous investigations into omega-3 FAD functionality have underscored the pivotal role of enzyme affinity and stability in determining enzymatic activity[15]. The affinity of enzyme molecules mainly refers to their ability to bind to substrates, while the stability of enzyme molecules is closely related to the spatial structure of their active regions[32]. PvFAD3, being a transmembrane protein[19], has posed challenges in *in vitro* purification, hindering the elucidation of its three-dimensional spatial structure through conventional crystallization methods. Predicting the protein's three-dimensional structure has also proven elusive through traditional means. In recent years, as protein and enzyme sequence data have burgeoned, the focus of functional analysis has shifted from conventional molecular biology experiments toward a hybrid approach that integrates experimental work with computer technologies. Such integration provides unprecedented insights into enzymatic mechanisms[24]. In this study, various software tools were employed to characterize the structural features, key binding sites with substrates, and hydrophobic transmembrane structures. The prediction results notably highlight the significant impact of ASP-104 on the affinity and stability of the PvFAD3 protein.

The genetic background and metabolic pathways of *S. cerevisiae* are well understood, and it is known for its rapid growth, easy mass production, and GRAS certification[33]. Previous studies have successfully achieved heterologous expressions of various recombinant proteins in *S. cerevisiae*, including Δ6 and Δ12 FADs[34,35]. Utilizing free linoleic acid as a substrate, the heterologous expression of linoleic acid isomerase has been shown to yield multiple conjugated linoleic acids[36]. Hence, exploring the catalytic activity differences between *PvFAD3* and m*PvFAD3* through heterologous expression in *S. cerevisiae* is a rational and effective approach. Through transgenic *S. cerevisiae* and GC-MS analysis, both *PvFAD3* and m*PvFAD3* expressions increased ALA contents, yet the former exhibited a significantly more substantial increase (Table 1). This result strongly supports the notion that ASP-104 positively influences PvFAD3 activity. This conclusion is further substantiated in transgenic *A. thaliana*. While both *PvFAD3* and m*PvFAD3* over-expressions in *AtFAD3*m enhanced ALA content in mature seeds, the impact of m*PvFAD3* expression was not as pronounced as that of *PvFAD3* expression (Table 2). Considering the outcomes of homologous modeling and molecular docking (Fig. 2), there is compelling evidence to speculate that ASP-104, as a key site in the PvFAD3 protein, positively influences the enzyme's activity.

Previous reports have proposed that the FAD3 protein is a low-temperature-active enzyme, suggesting that a lower culture temperature can enhance polyunsaturated FA content[37]. Indeed, the ALA content of *PvFAD3* transgenic yeast nearly doubled when the cultivation temperature was reduced from 30 °C to 20 °C (Table 1). However, the ALA content of m*PvFAD3* transgenic yeast did not exhibit similar responsiveness to the lower culture temperature. Conversely, a decrease in culture temperature for m*PvFAD3* transgenic yeast from 30 °C to 20 °C resulted in a 22.87% decline in ALA content (Table 1). Under the same temperature conditions, the ALA content in the *PvFAD3* was significantly higher than that in the m*PvFAD3*, and reducing the temperature further enhanced the statistical significance of this difference (Table 1). The radio tracer experiments have indicated that desaturase activity in *Brassica napus* comprises both temperature-independent basal desaturase activity, and low-temperature-induced desaturase activity[38]. It can therefore be assumed that ASP-104 may be involved in low-temperature-induced desaturase activity of PvFAD3 protein. To date, the molecular mechanisms underlying temperature modulation of FA profiles remain elusive.

Following FA biosynthesis, the saturated C16:0-ACP can either be hydrolyzed for C16:1 generation or be further elongated into C18:0-ACP, subsequently desaturated into C18:1, C18:2, and C18:3[20]. The intermediate metabolite, C16:0, generated during this process, exclusively chooses one metabolic pathway. Consistent with expectations, the *PvFAD3* transgenic yeast exhibited a significant reduction in C16:1 content (Table 1), suggesting that the *PvFAD3* expression could inhibit the desaturation of C16:0 to form C16:1. The inhibitory effect on C16:1 accumulation was more significant at lower temperatures. Because *Arabidopsis* seeds have very low C16:1 content[39], this inhibitory phenomenon has not been observed in *PvFAD3* transgenic plants. In addition, it is worth noting the extreme accumulation of C16:0 in *PvFAD3* transgenic yeast (Table 1). This can be explained considering that PvFAD3 inhibits the carbon flux towards C16:1. Interestingly, m*PvFAD3* expression did not significantly impact C16:0 and C16:1 content in yeast (Table 1). Whether the ASP-104 site of PvFAD3 protein can be related to the inhibitory role in C16:1 biosynthesis is still unclear and requires further verification. While it might be expected that 18-carbon chain FAs would notably increase in *PvFAD3* transgenic yeast, this did not occur, likely due to the limited capacity for C18:0 biosynthesis in yeast[40]. For example, in transgenic *PvFAD3 Arabidopsis*, despite the absence of significant C16:0 accumulation, there was a general increase in the contents of C18:1, C18:2, C18:3, C20:0, and C20:1.

Conclusions

Through the combination of bioinformatics analysis and computer simulation techniques, the ASP-104 of PvFAD3 protein was identified as a key site involved in protein stability and substrate binding. Substituting asparagine for aspartate at position 104 in yeast expression and *Arabidopsis* mutant complementation experiments unequivocally demonstrated a substantial reduction in

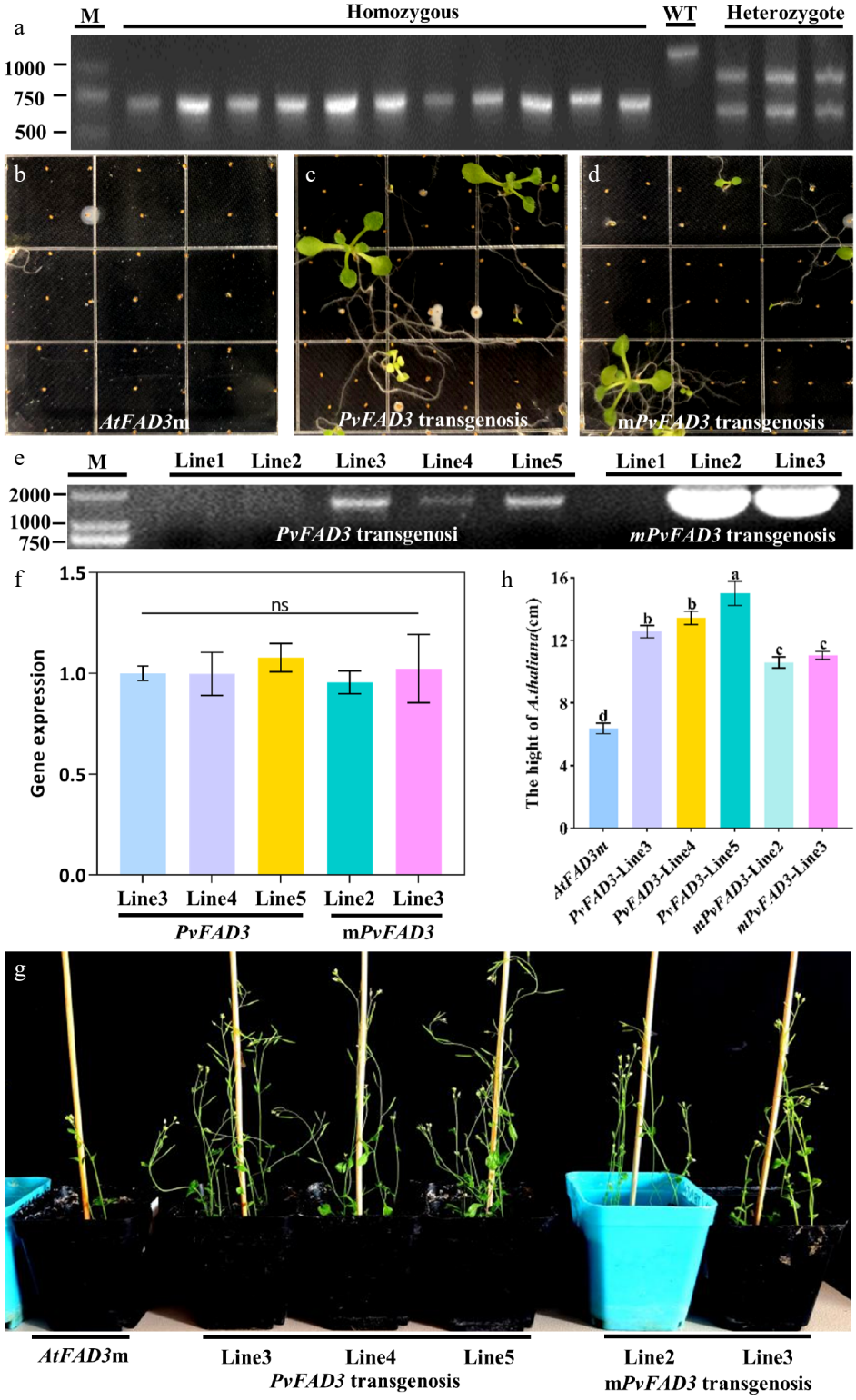

Fig. 5 Homozygous screening and genetic transformation of *AtFAD3*m. (a) *AtFAD3*m homozygote, WT and *AtFAD3*m heterozygote. (b) *AtFAD3*m seeding. (c) The transgenic *PvFAD3* positive seedlings of T_1 generation were screened for $Kana^+$ resistance. (d) The transgenic m*PvFAD3* positive seedlings of T_1 generation were screened for $Kana^+$ resistance. (e) PCR screening of transgenic plants. (f) RT-qPCR validation of transgenic plants. (g) When T_3 positive seedlings were transplanted into soil for 5 weeks, the growth state of transformed *PvFAD3* and m*PvFAD3* was significantly better than that of *AtFAD3*m. (h) Plant height statistics of *AtFAD3*m, *PvFAD3*, and m*PvFAD3*.

enzymatic activity for mPvFAD3, confirming the significance of ASP-104 as a key active site. This investigation enhances our comprehension of FAD3 enzyme activity, offering novel insights for the improvement of oil crop breeding and genetic engineering practices.

Author contributions

The authors confirm their contributions to the paper as follows: conceptualization, writing-original draft, methodology, validation, and formal analysis: Fu Y; methodology, validation, and formal

Table 2. Fatty acid compositions in *Arabidopsis* seeds.

Group	FA components (%)							
	C16:0	C18:0	C18:1	C18:2	C18:3	C20:0	C20:1	Total
*AtFAD3*m								
*AtFAD3*m - line1	1.62 ± 0.02^{d}	0.78 ± 0.04^{c}	2.79 ± 0.06^{de}	6.94 ± 0.06^{g}	0.21 ± 0.02^{b}	0.42 ± 0.02^{d}	3.03 ± 0.05^{f}	15.78 ± 0.08^{f}
*AtFAD3*m - line2	1.65 ± 0.06^{d}	0.80 ± 0.04^{c}	2.93 ± 0.06^{d}	7.51 ± 0.08^{e}	0.20 ± 0.03^{b}	0.44 ± 0.03^{cd}	3.15 ± 0.04^{e}	16.68 ± 0.16^{e}
*AtFAD3*m - line3	1.64 ± 0.03^{d}	0.80 ± 0.06^{c}	2.74 ± 0.04^{e}	7.25 ± 0.15^{f}	0.19 ± 0.01^{b}	0.40 ± 0.02^{d}	3.07 ± 0.05^{ef}	16.09 ± 0.26^{f}
PvFAD3 transfer								
PvFAD3 - line3	1.77 ± 0.06^{c}	0.79 ± 0.04^{c}	3.59 ± 0.19^{c}	9.78 ± 0.03^{b}	0.29 ± 0.02^{a}	0.55 ± 0.04^{b}	4.13 ± 0.07^{c}	20.90 ± 0.33^{c}
PvFAD3 - line4	1.75 ± 0.02^{c}	0.83 ± 0.06^{c}	3.62 ± 0.06^{c}	9.53 ± 0.06^{c}	0.30 ± 0.02^{a}	0.57 ± 0.02^{b}	4.12 ± 0.05^{c}	21.73 ± 0.12^{c}
PvFAD3 - line5	2.35 ± 0.06^{a}	1.10 ± 0.03^{a}	4.67 ± 0.13^{a}	10.96 ± 0.05^{a}	0.29 ± 0.03^{a}	0.65 ± 0.02^{a}	5.14 ± 0.05^{a}	25.17 ± 0.06^{a}
m*PvFAD3* transfer								
m*PvFAD3* - line2	1.76 ± 0.08^{c}	0.85 ± 0.03^{bc}	3.68 ± 0.09^{c}	8.49 ± 0.08^{d}	0.19 ± 0.01^{b}	0.47 ± 0.02^{c}	3.94 ± 0.08^{d}	19.40 ± 0.16^{d}
m*PvFAD3* - line3	1.92 ± 0.07^{b}	0.91 ± 0.02^{b}	4.08 ± 0.05^{b}	9.67 ± 0.10^{bc}	0.19 ± 0.02^{b}	0.53 ± 0.03^{b}	4.36 ± 0.06^{b}	21.66 ± 0.04^{b}

Different letters indicate significant differences ($p < 0.05$).

analysis: Wang Z; methodology, investigation: Ye L; validation: Deng G; formal analysis: Li K, Zou Y; writing-review and editing: Wang J; conceptualization, writing-review and editing, project administration, funding acquisition: Niu J. All authors reviewed the results and approved the final version of the manuscript.

Data availability

All data generated or analyzed during this study are included in this published article and its supplementary information files.

Acknowledgments

This work was supported by the National Natural Science Foundation of China (32401624). We thank BioRender (https://app.biorender.com/) as the schematic diagram in the graphical abstract was created using BioRender.com.

Conflict of interest

The authors declare that they have no conflict of interest.

Supplementary information accompanies this paper at (https://www.maxapress.com/article/doi/10.48130/tp-0025-0028)

Dates

Received 26 May 2025; Revised 28 July 2025; Accepted 24 August 2025; Published online 20 October 2025

References

1. Bocanegra Morales N, Galeano Garcia P. 2023. Chemical composition, fatty acid profile, and optimization of the sacha inchi (*Plukenetia volubilis* L.) seed-roasting process using response surface methodology: assessment of oxidative stability and antioxidant activity. *Foods* 12:3405
2. Istiandari P, Faizal A. 2025. Integrating *in vitro* cultivation and sustainable field practices of sacha inchi (*Plukenetia volubilis* L.) for enhanced oil yield and quality: a review. *Horticulturae* 11:194
3. Kittibunchakul S, Hudthagosol C, Sanporkha P, Sapwarobol S, Temviriyanukul P, et al. 2022. Evaluation of sacha inchi (*Plukenetia volubilis* L.) by-products as valuable and sustainable sources of health benefits. *Horticulturae* 8:344
4. Kodahl N, Sørensen M. 2021. Sacha inchi (*Plukenetia volubilis* L.) is an underutilized crop with a great potential. *Agronomy* 11:1066
5. Goyal A, Tanwar B, Kumar Sihag M, Sharma V. 2022. Sacha inchi (*Plukenetia volubilis* L.): an emerging source of nutrients, omega-3 fatty acid and phytochemicals. *Food Chemistry* 373:131459
6. Niu L, Li J, Chen MS, Xu ZF. 2014. Determination of oil contents in Sacha inchi (*Plukenetia volubilis*) seeds at different developmental stages by two methods: Soxhlet extraction and time-domain nuclear magnetic resonance. *Industrial Crops and Products* 56:187–90
7. Cordero-Clavijo LM, Mejía-Valdez D, Antunes-Ricardo M, Lazo-Vélez MA, Guajardo-Flores D. 2025. Evaluating sacha inchi (*Plukenetia volubilis*) oil stability and physicochemical properties: a comparison between conventional extraction and supercritical fluids. *Food Chemistry* 463:141132
8. Hu C, Xu X, Hu X, Zhang J, Shen L. 2025. Edible plant oils with high n-3/n-6 polyunsaturated fatty acids ratio prolong the lifespan of *Drosophila* by modulating lipid metabolism. *Food Chemistry* 474:143121
9. Bhatt DL, Libby P, Mason RP. 2025. Emerging pathways of action of eicosapentaenoic acid (EPA). *JACC Basic to Translational Science* 10:396–400
10. Yang W, Jia Y, Yang Y, Chen H, Zhou L, et al. 2025. Sacha inchi oil addition to hen diets and the effects on egg yolk flavor based on multi-omics and flavoromics analysis. *Food Chemistry* 475:143251
11. Gishini MFS, Kachroo P, Hildebrand D. 2025. Fatty acid desaturase 3-mediated α-linolenic acid biosynthesis in plants. *Plant Physiology* 197:kiaf012
12. Hoffmann M, Hornung E, Busch S, Kassner N, Ternes P, et al. 2007. A small membrane-peripheral region close to the active center determines regioselectivity of membrane-bound fatty acid desaturases from *Aspergillus nidulans*. *Journal of Biological Chemistry* 282:26666–74
13. Hernández ML, Jiménez-López J, Cejudo FJ, Pérez-Ruiz JM. 2024. 2-Cys peroxiredoxins contribute to thylakoid lipid unsaturation by affecting ω-3 fatty acid desaturase 8. *Plant Physiology* 195:1521–35
14. Wu D, Zhang K, Li CY, Xie GW, Lu MT, et al. 2023. Genome-wide comprehensive characterization and transcriptomic analysis of AP2/ERF gene family revealed its role in seed oil and ALA formation in perilla (*Perilla frutescens*). *Gene* 889:147808
15. Li X, Munir M, Zeng W, Sun Z, Chang X, et al. 2025. Characterization of fatty acid desaturase gene family in *Glycine max* and their expression patterns in seeds after *Fusarium fujikuroi* infection. *Frontiers in Plant Science* 16:1540003
16. Fan K, Qin Y, Hu X, Xu J, Ye Q, et al. 2023. Identification of genes associated with fatty acid biosynthesis based on 214 safflower core germplasm. *BMC Genomics* 24:763
17. Wu P, Zhang S, Zhang L, Chen Y, Li M, et al. 2013. Functional characterization of two microsomal fatty acid desaturases from *Jatropha curcas* L. *Journal of Plant Physiology* 170:1360–66
18. Chellamuthu M, Kumaresan K, Subramanian S. 2022. Increase in alpha-linolenic acid content by simultaneous expression of fatty acid metabolism genes in Sesame (*Sesamum indicum* L.). *Physiology and Molecular Biology of Plants* 28:559–72
19. Liu G, Wu Z, Shang X, Peng Y, Gao L. 2022. Overexpression of *PvFAD3* gene from *Plukenetia volubilis* promotes the biosynthesis of α-linolenic acid in transgenic tobacco seeds. *Genes* 13:450

20. Fu Y, Huo K, Pei X, Liang C, Meng X, et al. 2022. Full-length transcriptome revealed the accumulation of polyunsaturated fatty acids in developing seeds of *Plukenetia volubilis*. *PeerJ* 10:e13998
21. Delgado C. 2025. NICE approves gene editing therapy for patients with severe sickle cell disease. *BMJ* 388:r210
22. Deng X, Chen L, Hei M, Liu T, Feng Y, et al. 2020. Structure-guided reshaping of the acyl binding pocket of 'TesA thioesterase enhances octanoic acid production in *E. coli*. *Metabolic Engineering* 61:24–32
23. Zhou L, Tao C, Shen X, Sun X, Wang J, et al. 2024. Unlocking the potential of enzyme engineering via rational computational design strategies. *Biotechnology Advances* 73:108376
24. Zhang C, Feng Y, Zhu Y, Gong L, Wei H, et al. 2024. NAC4ED: A high-throughput computational platform for the rational design of enzyme activity and substrate selectivity. *mLife* 3:505–14
25. Wang M, Chen H, Gu Z, Zhang H, Chen W, et al. 2013. ω3 fatty acid desaturases from microorganisms: structure, function, evolution, and biotechnological use. *Applied Microbiology and Biotechnology* 97:10255–62
26. Bai Y, McCoy JG, Levin EJ, Sobrado P, Rajashankar KR, et al. 2015. X-ray structure of a mammalian stearoyl-CoA desaturase. *Nature* 524:252–56
27. Wang H, Klein MG, Zou H, Lane W, Snell G, et al. 2015. Crystal structure of human stearoyl–coenzyme A desaturase in complex with substrate. *Nature Structural & Molecular Biology* 22:581–85
28. Czechowski T, Stitt M, Altmann T, Udvardi MK, Scheible WR. 2005. Genome-wide identification and testing of superior reference genes for transcript normalization in *Arabidopsis*. *Plant Physiology* 139:5–17
29. Nayda NC, Thomas JM, Delaney CL, Miller MD. 2023. The effect of omega-3 polyunsaturated fatty acid intake on blood levels of omega-3s in people with chronic atherosclerotic disease: a systematic review. *Nutrition Reviews* 81:1447–61
30. Kim Y, Park Y. 2023. Intake of omega-3 polyunsaturated fatty acids and fish associated with prevalence of low lean mass and muscle mass among older women: analysis of Korea National Health and Nutrition Examination Survey, 2008–2011. *Frontiers in Nutrition* 10:1119719
31. Islam A, Takeyama E, Al Mamun M, Sato T, Horikawa M, et al. 2020. Green nut oil or DHA supplementation restored decreased distribution levels of DHA containing phosphatidylcholines in the brain of a mouse model of dementia. *Metabolites* 10:153
32. Su BM, Xu XQ, Yan RX, Xie Y, Lin J. 2019. Mutagenesis on the surface of a β-agarase from *Vibrio* sp. ZC-1 increased its thermo-stability. *Enzyme and Microbial Technology* 127:22–31
33. Sun W, Chen X, Bi P, Han J, Li S, et al. 2024. Screening and characterization of indigenous non-*Saccharomyces cerevisiae* with high enzyme activity for kiwifruit wine production. *Food Chemistry* 440:138309
34. Sun R, Gao L, Yu X, Zheng Y, Li D, et al. 2016. Identification of a Δ12 fatty acid desaturase from oil palm (*Elaeis guineensis* Jacq.) involved in the biosynthesis of linoleic acid by heterologous expression in *Saccharomyces cerevisiae*. *Gene* 591:21–26
35. Tanomman S, Ketudat-Cairns M, Jangprai A, Boonanuntanasarn S. 2013. Characterization of fatty acid delta-6 desaturase gene in Nile tilapia and heterogenous expression in *Saccharomyces cerevisiae*. *Comparative Biochemistry and Physiology Part B: Biochemistry and Molecular Biology* 166:148–56
36. He X, Shang J, Li F, Liu H. 2015. Yeast cell surface display of linoleic acid isomerase from *Propionibacterium acnes* and its application for the production of *trans*-10, *cis*-12 conjugated linoleic acid. *Biotechnology and Applied Biochemistry* 62:1–8
37. Chen L, Wang L, Wang H, Sun R, You L, et al. 2018. Identification and characterization of a plastidial ω-3 fatty acid desaturase EgFAD8 from oil palm (*Elaeis guineensis* Jacq.) and its promoter response to light and low temperature. *PLoS One* 13:e0196693
38. Williams JP, Khan MU, Mitchell K, Johnson G. 1988. The effect of temperature on the level and biosynthesis of unsaturated fatty acids in diacylglycerols of *Brassica napus* leaves. *Plant Physiology* 87:904–10
39. Nwafor CC, Li D, Qin P, Li L, Zhang W, et al. 2022. Genetic and biochemical investigation of seed fatty acid accumulation in *Arabidopsis*. *Frontiers in Plant Science* 13:942054
40. Yılmaz C, Ecem Berk Ş, Gökmen V. 2024. Effect of different stress conditions on the formation of amino acid derivatives by Brewer's and Baker's yeast during fermentation. *Food Chemistry* 435:137513